journal

J. Am. Ceram. Soc., 96 [8] 2598–2606 (2013)
DOI: 10.1111/jace.12407

Material and Elastic Properties of Al-Tobermorite in Ancient Roman Seawater Concrete

Marie D. Jackson,[‡] Juhyuk Moon,[‡,§] Emanuele Gotti,[¶] Rae Taylor,[‡] Sejung R. Chae,[‡] Martin Kunz,[‖] Abdul-Hamid Emwas,[††] Cagla Meral,[‡,‡‡] Peter Guttmann,[§§] Pierre Levitz,[¶¶] Hans-Rudolf Wenk,[‖‖] and Paulo J. M. Monteiro[‡,†]

[‡]Department of Civil and Environmental Engineering, University of California, Berkeley, California 94720

[§]Department of Mechanical Engineering, Civil Engineering Program, State University of New York, Stony Brook, New York 11794

[¶]CTG Italcementi S.p.A., Via Stezzano 87, Bergamo 24126, Italy

[‖]Lawrence Berkeley National Laboratory, 1 Cyclotron Rd, Mail Stop 15R348, Berkeley, California 94720

[††]King Abdullah University of Science and Technology, Thuwal 23955-6900, Kingdom of Saudi Arabia

[‡‡]Middle East Technical University, 06800 Ankara, Turkey

[§§]Helmholtz-Zentrum für Materialen und Energie GmbH, Institute for Soft Matter and Functional Materials, Berlin 12489, Germany

[¶¶]Université Pierre et Marie Curie, CNRS, Laboratory PECSA, Paris F-75005, France

[‖‖]Department of Earth and Planetary Science, University of California, Berkeley, California 94720

The material characteristics and elastic properties of aluminum-substituted 11 Å tobermorite in the relict lime clasts of 2000-year-old Roman seawater harbor concrete are described with TG-DSC and ^{29}Si MAS NMR studies, along with nanoscale tomography, X-ray microdiffraction, and high-pressure X-ray diffraction synchrotron radiation applications. The crystals have aluminum substitution for silicon in tetrahedral bridging and branching sites and 11.49(3) Å interlayer (002) spacing. With prolonged heating to 350°C, the crystals exhibit normal behavior. The experimentally measured isothermal bulk modulus at zero pressure, K_0, 55 ±5 GPa, is less than *ab initio* and molecular dynamics models for ideal tobermorite with a double-silicate chain structure. Even so, K_0, is substantially higher than calcium-aluminum-silicate-hydrate binder (C–A–S–H) in slag concrete. Based on nanoscale tomographic study, the crystal clusters form a well connected solid, despite having about 52% porosity. In the pumiceous cementitious matrix, Al-tobermorite with 11.27 Å interlayer spacing is locally associated with phillipsite, similar to geologic occurrences in basaltic tephra. The ancient concretes provide a sustainable prototype for producing Al-tobermorite in high-performance concretes with natural volcanic pozzolans.

I. Introduction

The crystal structure of ideal tobermorite and its associated poorly crystalline phase, calcium–silicate–hydrate (C–S–H), the cementitious binder of conventional portland cement concrete, has been the focus of research investigations published in *Journal of the American Ceramic Society* for 55 yr. These articles lay the foundation for understanding the crystal chemistry of tobermorite and C–S–H,[1–5] effects of alumina substitution for silicon in C–S–H and tobermorite,[6–11] crystallization processes of tobermorite in autoclaved concretes,[12,13] and mechanical properties of hydrous calcium silicates.[14–17] The present research describes material characteristics of 2000-yr-old Al-tobermorite synthesized at low temperature in ancient Roman seawater concrete in the context of these publications, and provides the first experimental measurements of the bulk modulus of the mineral.

Natural occurrences of pure tobermorite with 11.3 Å interlayer spacing occur rarely, mainly in hydrothermally altered limestone, along with plombierite, the same crystal but with 14 Å interlayer spacing.[6] Al-tobermorite,[7] where Al^{3+} substitutes for Si^{4+}, is the more common form of the mineral in geological environments,[18] where it forms mainly in hydrothermally altered basaltic rocks.[19,20] For example, 12 yr after the 1963–1967 eruptions at Surtsey, Iceland, Al-tobermorite had crystallized in basaltic tephra in subaerial and submarine hydrothermal environments at 70°C–150°C, in association with zeolite minerals, mainly analcite and phillipsite.[21] Some of the first laboratory syntheses of aluminum substituted tobermorite were produced with geologic materials—quicklime, kaolin, and microcrystalline quartz—at 110°C, with 4–7 wt% Al_2O_3 incorporated in the lattice of crystals with Ca/(Si + Al) = 0.8.[6] The (002) interlayer spacing in syntheses from alkali- and alumina-rich calcium silicate systems at 90°C–190°C increases with alumina content, up to 11.45 ± 0.02 Å.[7,18] The wide interlayer and the negative charge balance resulting from Al^{3+} substitution for Si^{4+} contributes to enhanced cation-exchange properties relative to ideal tobermorite for monovalent cations such as Cs^+, Rb^+, and K^+ and divalent cations such as Ba^{2+}, Sr^{2+}, Pb^{2+}, Cd^{2+}, Co^{2+}, Ni^{2+}, and Mg^{2+}.[9,10,22,23] Al-tobermorite could have important applications to high-performance concretes for nuclear and hazardous waste treatment and repository, if it could be synthesized in large quantities with environmentally sustainable methods and materials.

G. Scherer—contributing editor

Manuscript No. 32734. Received February 5, 2013; approved April 26, 2013.
†Author to whom correspondence should be addressed. e-mail: monteiro@ce.berkeley.edu

Ab initio and molecular dynamics simulations of the crystal structure and mechanical properties of ideal tobermorite provide a theoretical reference for the structure of C–S–H and its potential behavior as a crystalline binder in ordinary portland cement (OPC) concrete.[17,24–28] The poorly crystalline analog of Al-tobermorite, calcium–aluminum–silicate–hydrate (C–A–S–H), has shown good potential for improving the durability and service life of environmentally friendly concretes, where OPC is partially replaced with supplemental cementitious materials such as fly ash, blast-furnace slag, and natural volcanic ash pozzolan.[29–31] For example, crystallization of Al-tobermorite in autoclaved aerated concrete blocks using blast-furnace slag reduces processing time and increases compressive strength.[15,16] Although experimental determinations of the mechanical properties of tobermorite should provide new insights into its characteristics as a cementitious binder, the bulk modulus of neither the pure nor aluminous forms of the crystal has been measured.

Neither tobermorite nor Al-tobermorite has ever been observed in conventional concretes. In contrast, Al-tobermorite occurs ubiquitously in the relict lime clasts (Fig. 1) of ancient Roman concrete harbor installations, constructed between first century BCE and second century CE through the Mediterranean region.[32–35] The analyses presented in this article describe Al-tobermorite from a 10 m^2 by 5.7 m tall concrete block in Pozzuoli Bay, near Naples; they build on recent mineralogical decriptions.[35,37] Roman builders packed a pozzolanic mortar, composed of Flegrean Fields pumiceous volcanic ash pozzolan and fine pebble lime, and decimeter-sized chunks of zeolitic tuff from Flegrean Fields pyroclastic deposits that surround Pozzuoli Bay (*Baianus Sinus*) into a wooden form with a concrete facing submerged in seawater.[32,36] An adiabatic thermal model indicates that the maximum temperatures produced in the breakwater through heat evolved from the exothermic hydration of lime in seawater to form portlandite and the formation of C–A–S–H cementitious binder were less than 85°C, and the structure cooled to 14°C–26°C seawater temperatures in about 2 yr.[37] The environmental costs of producing the Roman seawater concrete were less than that of conventional concretes—lime calcined at about 900°C forms 5–9 wt% of the ancient concrete, while OPC klinker, kiln-fired at 1450°C, forms 10–25 wt% of typical concretes. Furthermore, the service life of the ancient structures in seawater is extraordinarily long-lived compared with modern concretes.[38] Langton and Roy[39] described data collected from ancient pozzolanic materials as predictors for the extended durability and longevity of modern borehole and shaft sealing materials. A classic experimental study by Sersale and Orsini[40] compared the pozzolanic reaction products of natural glasses, including Flegrean volcanic ash, and artificial glasses, including granulated blast-furnace slag, in saturated lime solution and described the tobermorite-like C–S–H and aluminous crystalline phases that developed in both systems.

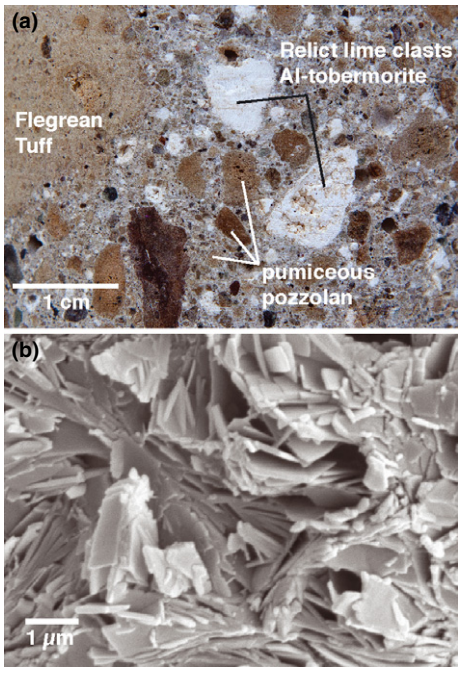

Fig. 1. Volcanic ash-hydrated lime mortar of the ancient Roman *Baianus Sinus* concrete, late first century BCE. (a) mortar of the BAI.2006.03 drill core. (b) Al-tobermorite crystals in a relict lime clast, scanning electron microscope, secondary electron (SEM-SE) image.

The purpose of this article is to describe the clusters of Al-tobermorite crystals that occur in relict lime clasts of the mortar of the *Baianus Sinus* concrete breakwater in terms of their bulk composition, thermal behavior, environments of Al^{3+} substitution for Si^{4+}, three-dimensional nanoscale morphology, and to derive elastic properties, measured as bulk modulus, from high-pressure X-ray diffraction experiments using synchrotron radiation. Fine crystals of Al-tobermorite also occur in the cementitious matrix of the ancient composite, shown by scanning transmission microdiffraction analyses with a monochromatic X-ray beam. Accessory minerals are associated with Al-tobermorite in these different environments, and reveal the diverse crystalline cementitious components of the very heterogeneous mortar fabric. C–A–S–H, however, is the principal cementitious binder, and Al-tobermorite forms less than 10 vol% of the pumiceous mortar.[33–35,37] The experimentally measured bulk modulus is compared with *ab initio* and molecular dynamics simulations of the crystal structure and mechanical properties of ideal tobermorite and the measured bulk modulus of C–A–S–H in slag concrete to provide a new reference for the mechanical behavior of Al-tobermorite as a potential cementitious binder in high-performance concretes formulated with natural volcanic pozzolans.

II. Materials, Methods, and Experimental Procedures

(1) Al-Tobermorite Specimen

The *Baianus Sinus* concrete breakwater was cored by the ROMACONS drilling program in 2006 (BAI.06.03) in collaboration with CTG Italcementi Laboratories in Bergamo, Italy. The mortar specimen studied here occurs 0.85 m below the surface of the breakwater, which now lies 3.45 m below present sealevel. Three Al-tobermorite specimens were removed from relict lime clasts 0.5–0.8 cm diameter in a 3 cm^2 area of the mortar. Magic Angle Nuclear Magnetic Resonance (MAS NMR) and nanoscale tomographic studies used one specimen, and high-pressure X-ray diffraction experiments used another, which were carefully picked through using a Leitz stereomicroscope to ensure purity. The thermal analysis used fragments from several relict lime clasts.

(2) Crystal Composition

The major element compositions of clusters of 3–5 μm-long Al-tobermorite crystals in relict lime clasts were acquired from a polished thin section of the mortar in the Electron Microprobe Laboratory at the Department of Earth and Planetary Science at UC Berkeley (Berkeley, CA) on a Cameca SX-51 electron microprobe equipped with five tunable wavelength dispersive spectrometers using the software, Probe for EPMA (v 8.69). Operating conditions were 40° takeoff angle, a beam energy of 15 keV, beam current of 10 nA, and a beam diameter of 1 μm. Counting time was 10 s for all elements. Oxygen was calculated by cation stoichiometry and included in the matrix correction. Secondary electron images (Fig. 1) were acquired from small particles of the mortar with a gold–palladium coating with a Zeiss EVOMA10 Scanning Electron Microscope at the Department of Earth and Planetary Science at UC Berkeley.

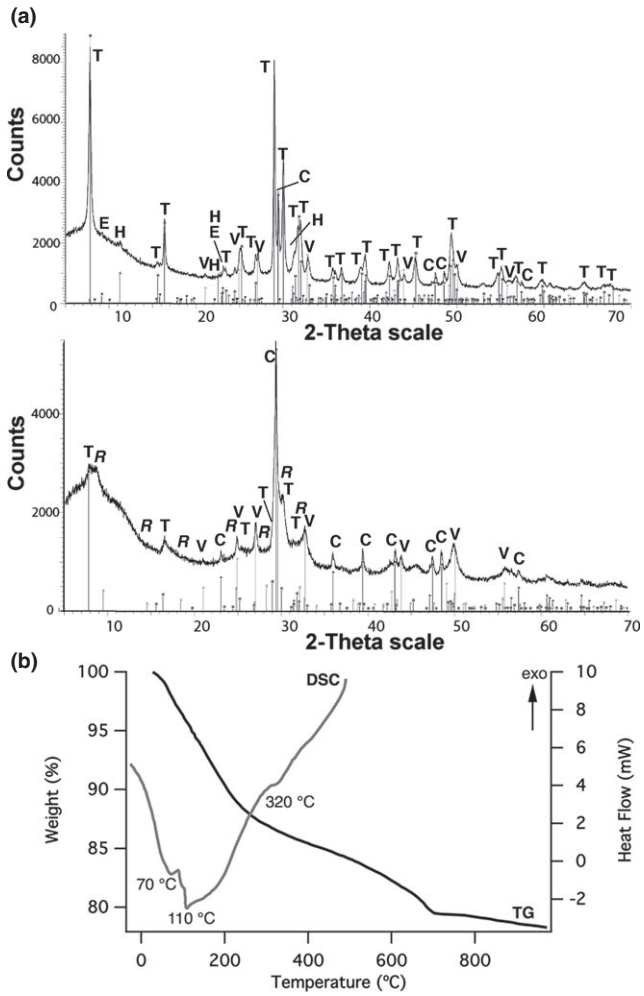

Fig. 2. Thermal analysis of *Baianus Sinus* Al-tobermorite in relict lime clasts. (a) powder X-ray diffraction pattern at ambient conditions, and after heating at 350°C for 20 h, with newly formed 9.3 Å riversidite and residual 11 Å Al-tobermorite. T: Al-tobermorite, C: calcite, E: ettringite, H: hydrocalumite, R: riversidite, V: vaterite. (b) results of thermal gravitational (TG) and differential scanning calorimetry analyses (DSC).

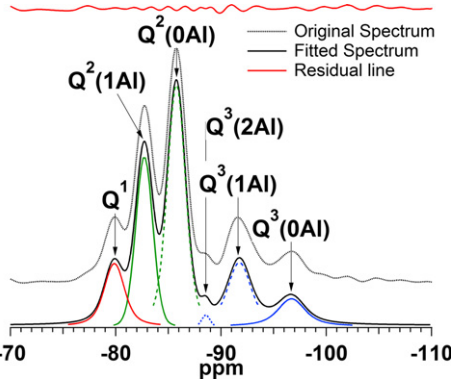

Fig. 3. Single-pulse ^{29}Si MAS NMR spectra of *Baianus Sinus* Al-tobermorite in a relict lime clast. The profiles include the original experimental spectrum, fitted peaks (labeled), and the residual after fitting (top: ×1). Table I shows the chemical shifts of the hydrate peaks (in ppm). Q^1, Q^2(0Al), and Q^3(0Al) peaks describe the connectivity of SiO_2 tetrahedra, where Q^1 are dimers or chain terminations, Q^2 are chain middle groups, and Q^3 are branching sites (after Jackson *et al.*[37]).

Table I. ^{29}Si MAS NMR, Chemical Shifts in ppm and Fractions of Anions Present in Each Environment in *Baianus Sinus* Al-Tobermorite

	Shift (ppm)	%
Q^1(0Al)	−79.86	12.51
Q^2(1Al)	−82.71	23.48
Q^2(0Al)	−85.76	39.64
Q^3(2Al)	−88.56	0.73
Q^3(1Al)	−91.75	15.58
Q^3(0Al)	−96.69	8.06

(3) TG-DSC and Conventional X-ray Diffraction

At CTG Italcementi Laboratories in Bergamo, Italy, thermal gravitational (TG) (Fig. 2) and Differential Scanning Calorimetry (DSC) analyses were performed with a simultaneous DSC–TGA instrument with 15 mg of the T2 specimen. The experimental conditions were: continuous heating from room temperature to 1000°C for the TG analysis and 500°C for the DSC analysis at a heating rate of 10°C/min; N_2-gas dynamic atmosphere (85 cm^3/min); alumina, top-opened crucible. X-ray powder diffraction (XRPD) analysis was performed with a Bruker D8-advance X-ray diffractometer, also at CTG Italcementi Laboratories (Bergamo, Italy) operating with a parafocusing geometry, equipped with Cu*K*a radiation, two sets of soller slits and a lynxeye™ PsD Detector (CTG Italcementi Laboratories). XRPD spectra were collected from 5° to 70° 2θ with a step of 0.02°/s, under ambient conditions and immediately after heating to 350°C for 20 h.

(4) ^{29}Si MAS NMR

The ^{29}Si MAS NMR analysis (Fig. 3, Table I) was performed at the Advanced Nanofabrication Imaging and Characterization Laboratories, King Abdullah University of Science and Technology, Saudi Arabia, with 50 mg of the finally ground T1 specimen packed into a 4 mm zirconia rotor and sealed at the open end with a Vespel cap.[37] The rotor was then spun at 14 kHz on a Bruker Ultrashield 400WB Plus with a 9.4 T magnet, operating at 79.495 MHz. The magic angle was set using KBr to 54.734°. Quantitative information on the fractions of silicon ions present in silicate tetrahedra with different connectivities were obtained by deconvolution of the single-pulse spectra. The spectra were fitted using the iterative fitting of the all the peaks to Voigt lineshapes using IgorPro 6.22A (Wavemetrics, Inc., Portland, OR).

(5) Nanoscale Tomography

Nanoscale computerized tomography (Fig. 4) was performed with the full-field soft X-ray microscope (TXM) beamline HZB-U41/1-TXM at the Berliner Elektronenspeicherring-Gesellschaft fu r Synchrotronstrahlung (BESSY) in Berlin, Germany.[41–45] Two-dimensional images were scanned under 280 eV incident beam energy, but for the tomographic analysis the incident energy was changed to 510 eV. Depending on optics settings the soft X-ray microscope can reach almost 10 nm spatial resolution. For this experimental setup, however, the best spatial resolution achievable was about 50 nm.[46] Global alignment using a cross-correlation between projection images taken at successive tilt angles collects tomographic data to produce a volumetric representation of the specimen. The three-dimensional reconstruction uses an algebraic method stabilized through a specific regularization technique.[47] From the binary image, a retraction graph without termini was computed.[48] This graph is composed of vertexes and links which locally and globally preserve the topology of the three-dimensional binary structure.[47,48]

(6) X-ray Microdiffraction

Identification of crystalline phases in the mortar fabric with X-ray microdiffraction (Fig. 5) at the micrometer scale was

determined at beamline 12.3.2 of the Advanced Light Source at the Lawrence Berkeley National Laboratory. This beamline uses a superconducting bending magnet as a source to deliver an X-ray spectrum ranging from 5 to 22 keV. Here, a monochromatic X-ray beam of 10 keV was focused to 2 (v) × 24 (h) μm diameter. The sample was placed in transmission mode[49] into the beam, with the detector 2θ at 39°. A Pilatus 1*M* area detector was placed at 150 mm to record Debye rings diffracted by the crystalline phases. The analyses determined the mineral assemblages in the cementitious matrix of a thin slice of mortar removed from a polished thin section, which had been previously characterized with petrographic analyses. Debye diffraction rings were radially integrated into intensity versus 2θ plots over an arch segment of 76° for 2θ 3°–30°.

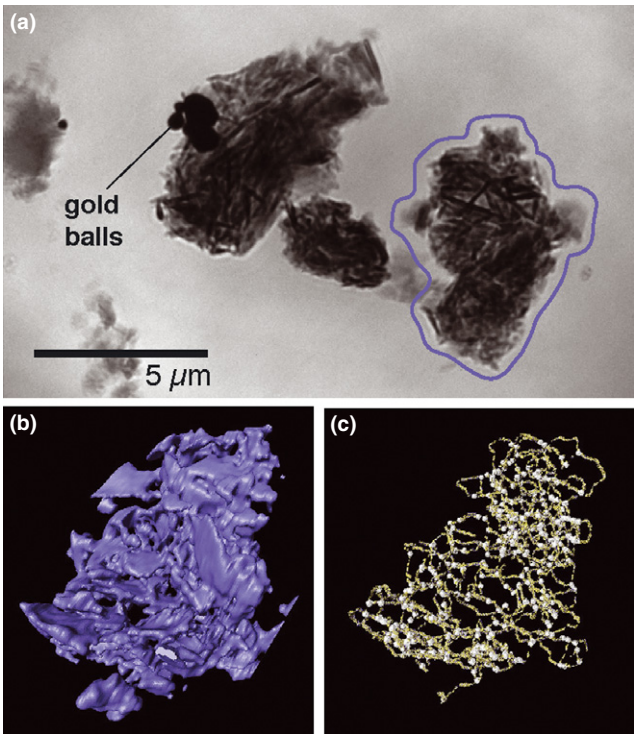

Fig. 4. Nanotomographic reconstruction of *Baianus Sinus* Al-tobermorite crystal clusters in a relict lime clast, soft X-ray microscope. (a) typical XM transmission image obtained with 280 eV incident X-ray. (b) high-resolution nanotomography reconstruction obtained with 510 eV incident X-ray. (c) associated topological skeleton.

(7) Synchrotron Based High-Pressure X-ray Diffraction

Ambient phase identification and high-pressure X-ray diffraction experiments (HPXRD) of the S1 powdered specimen were determined at beamline 12.2.2 of the Advanced Light Source at the Lawrence Berkeley National Laboratory[50] using a synchrotron monochromatic X-ray beam with a 0.6199 Å (20 keV wavelength) (Figs. 6 and 7, Tables II and III). The Al-tobermorite specimen was finely ground and mixed with a silicone oil (composed of polysiloxane chains with methyl and phenyl groups) and a few chips of ruby, and placed into a sample chamber 180-μm in diameter and 75-μm thick within a steel-gasketed diamond anvil cell. The specimen was equilibrated for about 20 min at each pressure. Diffraction patterns were collected at 600 s exposure times with 237.8 mm sample to detector distance. The pressure was measured off-line using the ruby fluorescence technique.[51] All two-dimensional X-ray images were radially integrated to give calibrated XPRD patterns using the fit2d program (Fig. 6).[52] Eleven diffraction peaks were used to calculate lattice parameters (Fig. 7). Changes in lattice parameters and unit cell volume were computed using the XFit and Celref programs (Fig. 6, Table II).[53,54]

III. Experimental Results

Descriptions of the Al-tobermorite in the *Baianus Sinus* concrete include material characteristics previously described for

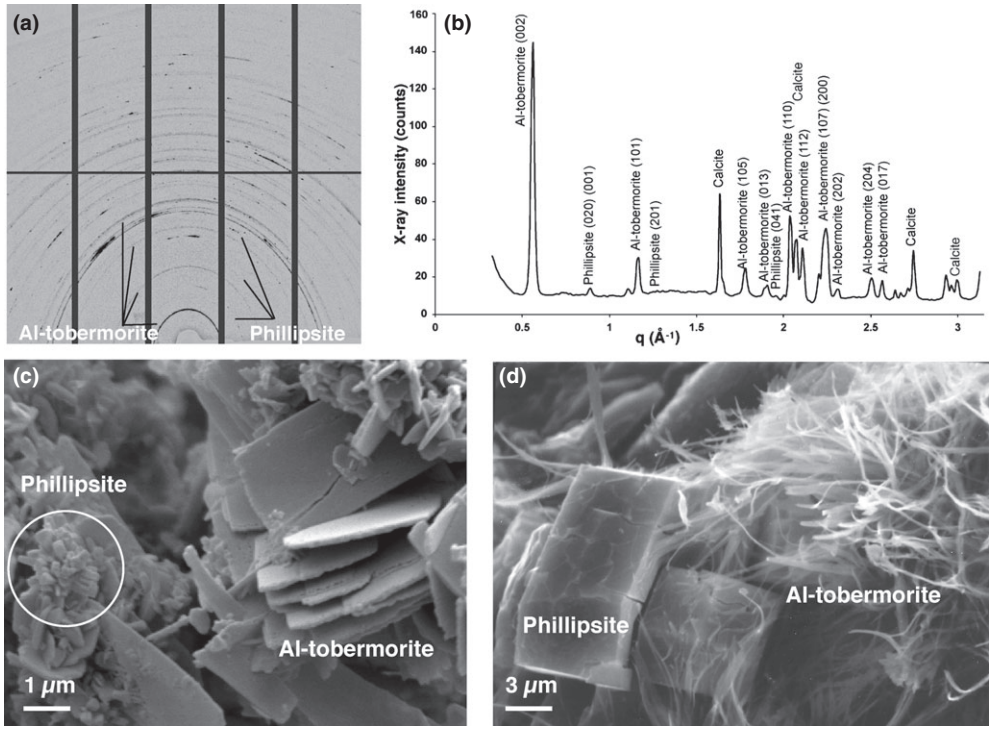

Fig. 5. Al-tobermorite and phillipsite in the cementitious matrix of the *Baianus Sinus* mortar. (a) Pilatus 1*M* area detector and Debye rings diffracted by the crystalline phases in monochromatic (10K eV) X-ray micro-diffraction experiments. (b) associated d-spacings and intensities of the Al-tobermorite, phillipsite, and calcite phases. SEM-SE images showing (c) a phillipsite rossette that has crystallized on a platy Al-tobermorite crystal, and (d) phillipsite and Al-tobermorite in the submarine Surtsey tuff, Iceland that crystallized at about 150°C in a 1979 drill core.

Table II. Experimental Pressures and Measured Lattice Parameters and Unit Cell Volumes of *Baianus Sinus* Al-Tobermorite

P (GPa)	*V* (Å^3)	*a* (Å)	*b* (Å)	*c* (Å)
Ambient	474 (1)	5.606 (9)	3.69 (9)	22.87 (6)
0.1 (1)	473.7 (5)	5.59 (2)	3.69 (2)	22.90 (1)
0.6 (1)	469.1 (8)	5.57 (4)	3.68 (3)	22.82 (2)
0.9 (1)	465 (1)	5.57 (8)	3.68 (7)	22.70 (4)
1.8 (2)	461 (1)	5.55 (9)	3.67 (8)	22.64 (5)
2.7 (2)	453 (4)	5.53 (3)	3.65 (1)	22.4 (1)
3.9 (3)	444 (6)	5.51 (5)	3.62 (2)	22.1 (1)
5.4 (4)	438 (7)	5.52 (6)	3.61 (3)	21.9 (1)
6.2 (4)	433 (8)	5.49 (7)	3.62 (3)	21.8 (1)

geological occurrences and laboratory syntheses, as well as experimental measurements of the elastic properties of the mineral.

(1) Material Characteristics

(A) Composition: Al-tobermorite crystals in relict lime clasts (Fig. 1) have Ca/(Si + Al) = 0.8, high Al/(Si + Al) = 0.16–0.17, and low silica contents relative to crystals in geologic environments. A typical EPMA analysis yields 37.93 SiO_2, 6.41 Al_2O_3, 0.06 MgO, 35.02 CaO, 0.65 Na_2O, 1.04 K_2O, 18.88 H_2O. C–A–S–H in the dissolved perimeters of relict lime clasts also have average Ca/(Si + Al) = 0.8. The XRPD analysis of the Al-tobermorite specimen subjected to thermal analysis (Fig. 2) shows weak traces of hydrocalumite and ettringite. These occur in submillimeter-sized microstructures surrounding the relict lime clasts, which sequester chloride in hydrocalumite and sulfate in ettringite.[35] There is also secondary alteration to calcite and vaterite.

(B) Thermal Behavior: After heating to 350°C for 20 h, the hydrocalumite and ettringite peaks disappear, calcite and vaterite persist, and the 11 Å peak reflecting the Al-tobermorite (002) interlayer spacing decreases in intensity but remains present, as do other tobermorite peaks [Fig. 2(a)]. The heating process produced riversidite with 9.3 Å interlayer spacing; this indicates dehydration and shrinkage in the **c** crystallographic direction. Thus, both anomalous and normal tobermorite are present[19] and perhaps, also, an amorphous component. The steep endothermic curve in the DSC diagram [Fig. 2(b)] indicates release of adsorbed and bound water in Al-tobermorite (and minor amounts of hydrocalumite and ettringite) at <110°C, and additional release of bound water at 320°C. The TG curve records about 22% weight loss overall during heating from 25°C to 1000°C, with about 9.5% loss from 25°C to 200°C, 4% loss at 200°C–320°C, and 8.2% loss at 320°C–1000°C. The steep drop in the DSC curve may indicate dehydration and formation of the riversidite crystals. Although there is a trace of endothermic decomposition of secondary calcite at about 695°C, the steady decline of the TG curve at 700°C–1000°C indicates that recrystallization to a high-temperature phase with a smaller *c* axis[52] or to wollastonite[19] did not occur. Thermal shrinkage of the tobermorite lattice to 9 Å riversidite occurs when calcium cations exist in the structural cavities of the interlayer.[55] The bonding environments of these zeolitic Ca cations have important implications for the thermal stability of various Al-tobermorite structures.[8] The collapse of layered crystalline structure in at least some of the *Baianus Sinus* crystals thus seems to reflect rather stable Ca^{2+}, Na^+, and K^+ binding environments with heating.

(C) Silicon Bonding Environments: ^{29}Si MAS NMR study demonstrates that alumina tetrahedra (Al_2O_4) occur in the silicate chain, Q^2(1Al), and branch, Q^3(1Al) or Q^3(2Al), positions of the layered *Baianus Sinus* Al-tobermorite structure (Fig. 3).[37] The high intensity of the Q^2 peaks relative to

Table III. Crystallographic Data and Experimentally Measured Bulk Modulus of *Baianus Sinus* Al-Tobermorite, Compared with Theoretical Calculations for Pure 11 Å Tobermorite[24,25] and the Measured Bulk Modulus of C–A–S–H.[69] Shahsavari *et al.*[17] and Manzano *et al.*[27] determined elastic constants by calculating forces for strained configurations. Here, the isothermal bulk modulus, K_0, was determined from Birch-Murnaghan equation of state parameters, truncated at second order ($K_0' = 4$).[66] The large error range comes from variations in the refined unit cell at each pressure, particularly the c lattice parameter. In the Hamid model silica tetrahedra attached to Ca–O layers form independent chains, while in the Merlino model silica tetrahedra chains are covalently connected. Numbers in brackets refer to references cited

		11 Å Tobermorite				Tobermorite-like C–S–H		C–A–S–H
Material properties	*Baianus Sinus* this study		Hamid model[17]		Merlino model[17,27]	Hamid model[26]	Defect Merlino model[28]	Slag cement[69]
Chemical formula	Ca:Si:Al 1:1:0.2	$Ca_6Si_6O_{18}$ $\cdot 2H_2O$	$Ca_5Si_6O_{16}(OH)_2$ $\cdot 2H_2O$	$Ca_4Si_6O_{14}(OH)_4$ $\cdot 2H_2O$	$Ca_4Si_6O_{15}(OH)_2$ $\cdot 5H_2O$	C–S–H	$(CaO)_{1.65}(SiO_2)$ $\cdot(H_2O)_{1.75}$	C–A–S–H
Ca/(Si + Al)	0.8	1	0.83	0.67	0.66	1	0.83	0.72
Crystal system	Imm2, $Z = 2$		Imm2, $Z = 2$		F2dd, $Z = 8$	n.d.	n.d.	n.d.
Basal spacing (Å)	11.49 (3)		11.3895		11.2425	12.5	11.9	11.39 (2)
Volume (Å^3)	474 (1)	470.4	464.2	459.0	479.8 (5)	n.d.	484.4	470.29
Bulk modulus (GPa)	55 (5)	60 (5)	58 (3)	52 (2)	66 (1) 74	71.8	49 (2)	35 (3)

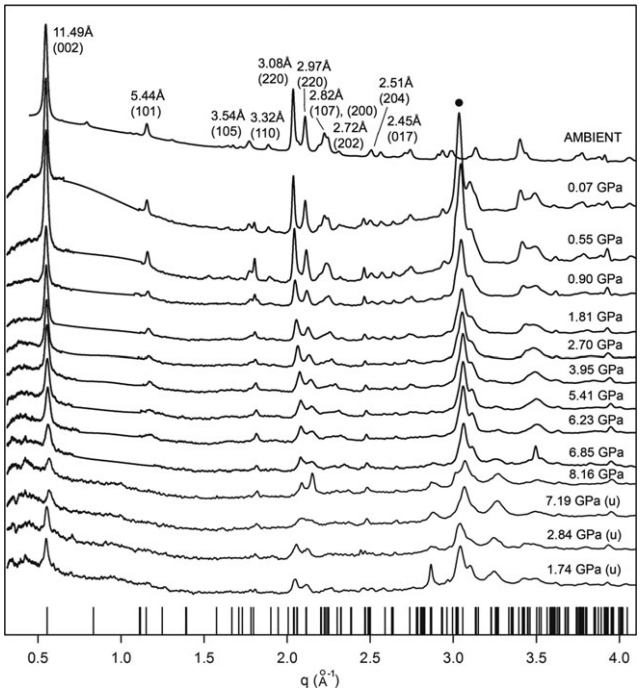

Fig. 6. Integrated powder X-ray diffraction patterns of *Baianus Sinus* Al-tobermorite as a function of pressure. The right side of the y-axis indicates hydrostatic pressure in the diamond anvil cell [(u), unloading]. The vertical lines on the *x*-axis are diffraction peaks from Merlino *et al.*[25] The top diffraction pattern was measured at ambient conditions, and the others are loading and unloading diffraction patterns with the silicone oil pressure-transmitting medium. Newly emerging peaks (•) in the post-compression sample are from ruby chips.

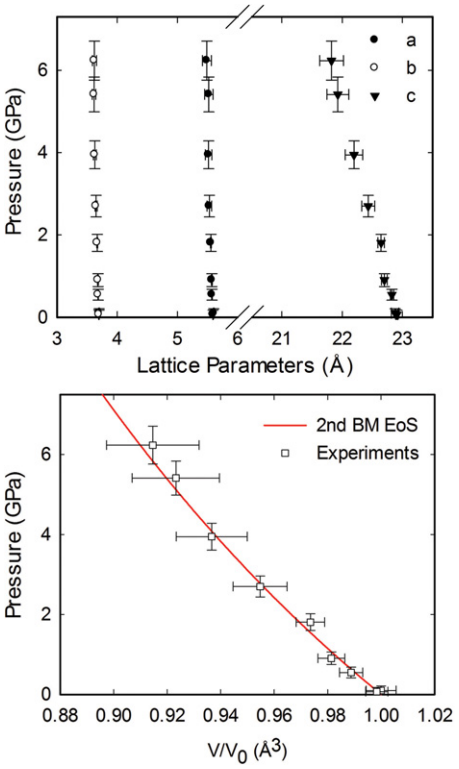

Fig. 7. Pressure-dependent behavior of the *Baianus Sinus* Al-tobermorite unit-cell volume normalized to the ambient volume. The second order Birch-Murnaghan equation of state fitting gives the bulk modulus K_0 = 55 ±5 GPa.

the Q^1 peak indicates long-chain lengths.[30,56,57] The higher intensity of Q^2(0Al) relative to Q^2(1Al) indicates that Al^{3+} is present in the bridging, or paired, tetrahedra, of the silicate chains, but that Si^{4+} dominate. In the branching tetrahedral sites that join the silicate chains, however, the higher intensity of Q^3(1Al) relative to Q^3(0Al) indicates that Al^{3+} is more common than Si^{4+}.[30,56–58] These results are confirmed with ^{27}Al MAS NMR, in which the 65.63 peak has substantially higher intensity than the 57.70 peak.[37] A small shoulder on the Q^2(0Al) peak at −88.57 ppm corresponds to Q^3(2Al), with a downfield shift of 9 ppm from Q^3(0Al) due to aluminum shielding.[16]

Deconvolution of these results provides quantitative information on the fractions of silicon ions present in silicate tetrahedra with different connectivity (Table I). The relative intensity, determined through an iterative process of fitting the observed peaks to the profiles of Fig. 3, is used to calculate the mean chain length (MCL) following Richardson and Groves.[59] MCL is 13.97, relatively high in comparison to C–S–H in OPC, but similar to C-A-S-H in high content blast furnace slag concretes[60] and the overall Q^2/Q^3 ratio is 2.59. In the ^{29}Si MAS NMR literature, the ratio of Q^2 to Q^1 peak intensity is frequently taken as a representation of MCL for tobermorite-like C–S–H. However, Q^2/Q^1 of the deconvoluted results gives MCL of only 5.07. Al-tobermorite crystals in the *Baianus Sinus* relict lime clasts [Fig. 2(a)] and cementitious matrix [Fig. 5(c)] are not thread-like C–S–H fibers, but, rather, uniformly thin plates with $b > c \gg a$, and orthorhombic symmetry (Table III). If this platey morphology and the Q^3 linkages of the double silicate chain structure that extends in the *c* direction are taken into account, then Q^2/Q^1 multiplied by a Q^2/Q^3 scale factor gives a possible MCL estimate of 13 (Fig. 3, Table I). Considering the study of Wieker *et al.*[61] the Q^2/Q^3 ratio would suggest a Ca/Si ratio close to 0.9, almost identical to the 0.92 measured through EPMA analysis.[37]

(D) Nanoscale Structure of Al-tobermorite Clusters: A grey-level nanoscale tomographic reconstruction of clusters of Al–tobermorite crystals from a relict lime clast [Fig. 4(a) and (b)] shows both platey and elongated 1–2 μm crystals typical of geological 11 Å tobermorite[19] and laboratory syntheses.[1] The three-dimensional skeleton graph [Fig. 4(c)] can be characterized by a connectedness number, *C*, which is an intensive topological characteristic related to the number of irreducible paths per vertex. *C* is defined as $C = -(\alpha_0 - \alpha_1)/\alpha_0$, where α_0 is the number of vertexes (isolated or not), and α_1 is the number of links.[47,48] It is related to the average number of links per vertex, *Nc*, through the equation $Nc = 2(1 + C)$.[47]

The connectedness number computed for the Al-tobermorite cluster of Fig. 4(c), with a 15.5 nm voxel dimension and an average 3.3 links per vertex, is 0.65. This indicates a well-connected solid mass [Fig. 4(b) and (c)], as a negative value of *C* is associated with a strongly disconnected network, below its percolation threshold, and a well-connected network has a $C > 0.5$. The calculated porosity, 52%, is qualitative, and due to a relatively basic segmentation protocol, this value could be overestimated. This is similar, however, to 36%–39% porosity in Al-tobermorite with Ca/(Al + Si) = 0.8 in autoclaved aerated concrete.[12] The imaging demonstrates that the Al-tobermorite crystals are at least two orders of magnitude longer than poorly crystalline, tobermorite-like C–S–H (I), about 3.5 nm, determined through X-ray pair distribution functions.[62]

(E) Cementitious Matrix: Al-tobermorite also occurs in the cementitious binding matrix of the pumiceous mortar of the ancient concrete, as 2–5 μm platy crystals (Fig. 5). Debye diffraction rings measured with the monochromatic X-ray micro-diffraction beam [Fig. 5(a)] show strong continuous reflections from Al-tobermorite with (002) interlayer spacing 11.27 Å; the low rugosity indicates a nano-crystallized grain size. The 3.20 (100), 7.16 (68), and 7.16 (53) reflections of phillipsite[63] are present in very restricted

segments of the diffraction cone, however, indicating a strong preferred orientation [Fig. 5(a)]. This explains the absence of other nominally strong reflections, such as (−201) at 4.96 Å [Fig. 5(b)]. An SEM-SE image of this assemblage shows submicrometer-sized phillipsite that has crystallized on 2–4 μm plates of Al-tobermorite [Fig. 5(c)]. In addition to relicts of unreacted phillipsite present in the pumiceous pozzolan,[34] authigenic phillipsite with potassic compositions has been described in pores of the ancient mortar fabrics in seawater harbor concretes from Tuscany, Italy, and Caesarea, Israel.[33,35] This may be the result of low-temperature alteration of residual alkali-rich volcanic glass in the seawater concrete system at pH 9–10, after portlandite has been consumed.[35,64] Association of Al-tobermorite with phillipsite also occurs in the glassy matrix of the Surtsey tuff [Fig. 5(d)], after twelve years of hydrothermal alteration at 70–150°C.[21] Alteration of basaltic glass on the southeast flank of Mauna Loa at 1.4 km depth and 15°C also has produced calcium silicate crystals in association with potassic phillipsite.[65]

(2) Elastic Properties

Experimental measurements of the elastic properties of *Baianus Sinus* Al–tobermorite isolated from relict lime clasts are described and then compared with theoretical models of the bulk modulus of ideal tobermorite and C–S–H, to show how pervasive aluminum substitution, measured through ^{29}Si MAS NMR studies (Fig. 3) influences material properties.

(A) Analytical Results: The pressure-normalized volume data were fitted by a Birch-Murnaghan equation of state,

$$P = \frac{3}{2}K_0\left[(V/V_0)^{\frac{-7}{3}} - (V/V_0)^{\frac{-5}{3}}\right]\left[1 + \frac{3}{4}(K_0' - 4)\left((V/V_0)^{\frac{-2}{3}} - 1\right)\right]$$

where V is the unit cell volume, V_o is the initial unit cell volume at ambient pressure, P is the applied pressure, K_0 is the bulk modulus at zero pressure, and K_0' is the derivative of bulk modulus at zero pressure.[66] A weighted linear least-squares fit to the equation with fixed $K_0' = 4$ was applied to consider both pressure and volume error.[67] Strong X-ray reflections for (002) at 11.49 Å, (110) at 3.08 Å, and (112) at 2.97 Å at ambient pressure indicate a high degree of crystallinity (Fig. 6). At ambient pressure the interlayer spacing is 11.49(3) Å, where the numbers in parentheses here, and in Table II, are standard deviations from the measured experimental values. There are refined orthorhombic *Imm*2 lattice parameters of a = 5.60(9) Å, b = 3.69(9) Å, and c = 22.87 (6) Å, and a computed bulk modulus, K_0 = 55 ± 5 GPa, with R2 = 0.99 fitting convergence. With increasing pressure, changes in a and b lattice parameters are small, but the c lattice parameter contracts.

(B) Comparison with Models of Ideal Tobermorite: Theoretical calculations indicate that the bulk modulus of ideal tobermorite with condensed double-silicate-tetrahedra chains, 67–74 GPa, should be less compressible than that with independent single chains, 53–61 GPa (Table III).[24–28] The measured bulk modulus of *Baianus Sinus* Al–tobermorite (Table II) lies within the range of *ab initio* calculations for ideal tobermorite with single silicate chains.[24] However, Q^3(1Al), Q^3(0Al), and Q^3(2Al) bonding environments (Fig. 3) indicate tetrahedral linkages across the silicate interlayer and therefore, crystals with double-silicate-tetrahedra chains.[30,55,56] Al–O bond lengths are about 8%–10% longer than Si–O bond lengths and Al–O binding energy is less than Si–O,[68] so pervasive Al^{3+} substitution for Si^{4+} in chain and branching sites should result in weakened bonds at bridging and branching sites, as shown by vibratory milling experiments[16] and increased (002) interlayer spacing.[18] Similarly, Al^{3+} substitution in the defect tobermorite model[17] should decrease the bulk modulus compared with the Merlino model (Table II).[55] This is consistent with the experimental results, and with molecular dynamics simulations of Al-tobermorite,[11] in which substitution of Si^{4+} with Al^{3+} and Na^+ produces increased interlayer thickness and decreased elastic modulus, with increasing Al/Si. The wide interlayer of the *Baianus Sinus* Al-tobermorite presumably provides cavities for Na^+ and K^+ cations derived from reaction between the alkali-rich volcanic ash and seawater-saturated lime, and contributes to charge balancing and stability.[9,10,18,22] These features, however, increase compressibility relative to ideal tobermorite with 11.3 Å spacing. Even so, the measured bulk modulus is substantially higher than measurements of C–A–S–H in alkaline-activated slag concrete, 35 ± 3 GPa, and C–S–H, 34 ± 7 GPa[69]; and computational models for tobermorite-like C–S–H with finite chain lengths, 21–29 GPa.[27] This suggests that future applications of Al-tobermorite as a cementitious binder could increase concrete mechanical performance relative to poorly crystalline C–A–S–H.

IV. Discussion

Measurements of the crystallographic parameters and bulk modulus, K_0, of *Baianus Sinus* Al-tobermorite (Figs. 6 and 7, Table I and II) provide an exceptionally unique guidepost for predicting the long-term material properties of Al-tobermorite as a cementitious binder. The aluminous, orthorhombic form of the mineral with Ca/(Si + Al) = 0.8 in the ancient concrete, has (002) interlayer spacing of 11.49 (3) Å and experimentally measured bulk modulus, 55 ± 5 GPa, substantially higher than the C–A–S–H of slag concrete[69] but lower than *ab initio* calculations[17] and molecular dynamic simulations[27] for pure, ideal tobermorite. The differences likely arise from the presence of additional cations, Al^{3+} and small amounts of Na^+ and K^+ in the *Baianus Sinus* Al-tobermorite crystal structure, in addition to thermal vibration effects in the real crystals.[70] The bonding environments of Al^{3+} substitution for Si^{4+} in the crystal lattice described by NMR studies indicate long silicate chain lengths and pervasive tetrahedral cross-linkages of the silicate interlayer with overall Q^2/Q^3 about 2.59 (Fig. 3). Long silicate chain lengths and low Ca/(Si + Al) = 0.8 suggest a high degree of polymerization and Si^{4+} binding energy, which typically produce strong cement paste in conventional concretes.[59] The Al-tobermorite may have developed longer chain lengths over time, similar to C–A–S–H in ground granulated blast-furnace slag concretes.[59] With heating, some crystals dehydrate and collapse to a 9 Å riversidite structure (Fig. 2). This indicates a crystal structure that evidently crystallized at low temperature, <85°C, based on a thermal model of the *Baianus Sinus* breakwater,[37] and remained stable at seawater temperatures for a very long period of time, but may exhibit normal dehydration behavior at the elevated temperatures of certain high-performance concrete applications.

The presence of Al-tobermorite in the matrix of the pumiceous mortar (Fig. 5) indicates that the crystals do not only form in relict lime clasts but also act as a cementitious binder in the ancient composite. The (002) interlayer spacing, about 11.27, is smaller than that of crystals in the relict lime clasts, perhaps the result of a less aluminous compositions. Other *d*-spacings and intensities are largely the same. Crystallization of phillipsite on Al-tobermorite plates [Fig. 5(c)] indicates that cementitious processes may continue after hydration of portlandite and the C–A–S–H binder, perhaps associated with hydration of volcanic glass in the seawater environment.[63] A similar mineral assemblage developed in the 12-yr-old Surtsey tuff, but at 70°C–150°C hydration temperatures [Fig. 5(d)]. Both Al-tobermorite and phillipsite have cation-exchange capacities for heavy metals and radionucleides.[9,10,22,23,71]

The ancient Roman syntheses of Al-tobermorite in the seawater mortars have relevance to new advancements in environmentally friendly, high-performance concretes. For example,

the large interlayer spacing relative to ideal tobermorite,[17,25–27] and the high, experimentally measured bulk modulus of the aluminum-substituted crystals relative to C–A–S–H,[69] are particular properties that should inform future durability strategies based on the compositional aspects of a variety of blended cementitious materials. In addition, the maritime concrete design mix contains <10 wt% lime,[37] which is calcined at 850°C–900°C, far lower than the 1450°C required for OPC clinker. This suggests that certain lime-based cementious composites formulated with pyroclastic rock may produce lower CO_2 emissions relative to OPC concretes, and also crystallize Al-tobermorite under certain conditions. Furthermore, Al^{3+} and Na^{+} substituted tobermorite has the potential to sequester cations such as cesium,[23] and Al-tobermorite may contribute, along with zeolite cements, to long-term clogging of pore space in concrete waste repositories.[72] Current efforts to encapsulate hazardous wastes in concrete containers have mainly considered blast-furnace slag cement designs, so the Roman maritime concrete prototype, which developes both Al-tobermorite and phillipsite (Fig. 5) may provide new perspectives for experimentation with lime-pyroclastic rock concrete designs. The investigations presented here, and the proven durability of the ancient Roman seawater mortar formulation, suggest that volcanic tephra may be a viable alternative to inform the synthesis of crystalline Al-tobermorite and potentially maximize silicate chain lengths, silicate binding energy, and cation-exchange capabilities in exceptionally long-lived cementitious systems.

IV. Conclusions

Synchrotron-based high-pressure X-ray diffraction (HPXRD) experiments show how pervasive alumina substitution for silicon influences the elastic properties Al-tobermorite, isolated from a relict lime clast in a massive Roman concrete breakwater, which was constructed with pyroclastic rock and lime hydrated in the seawater in the Bay of Pozzuoli during first century BCE. Al^{3+} in the chain and branching sites of a double-silicate-tetrahedra chain crystal structure produced a large interlayer spacing, 11.49(3) Å, and a computed bulk modulus, $K_0 = 55 \pm 5$ GPa, which is lower than theoretical calculations of ideal tobermorite. This is, perhaps, because Al^{3+} substitution for Si^{4+} produces increased interlayer spacing and weakened bonds at bridging and branching sites. However, K_0 is substantially higher than experimental measurements of modern C–A–S–H cementitious binder. Al-tobermorite also occurs in the cementitious matrix of the pozzolanic mortar, in association with phillipsite. The proven endurance of the crystals in the seawater environment for 2000 yr indicates exceptionally high durability in a complex pozzolanic concrete composite, on a par with the stable rock forming cementitious minerals of the earth's crust.

Acknowledgments

This research was supported by Award No. KUS-l1-004021, from King Abdullah University of Science and Technology (KAUST). Data were acquired at beamlines 12.2.2 and 12.3.2 at the Advanced Light Source at the Lawrence Berkeley Laboratories, supported by the Director of the Office of Science, Department of Energy, under Contract No. DE-AC02-05CH11231, and the Advanced Nanofabrication Imaging and Characterization Laboratories at King Abdullah University of Science and Technology. We thank CTG Italcementi researchers and staff, especially B. Zanga, in Bergamo, Italy; G. Vola at Cimprogetti S.p.A., Dalmine, Italy; S. Clark at the 12.2.2 beamline; and N. Tamura at the 12.3.2 beamline; and the ROMACONS drilling program: J. P. Oleson, C. Brandon, R. Hohlfelder. T. Teague, D. Hernandez, C. Hargis, I. A. Delaney, and B. Black provided research support. We thank J. G. Moore, M. Sintubin, G. Sposito, P.-A. Itty, and J. Kirz for critical discussions, and three anonymous reviewers whose comments improved the manuscript.

References

[1]G. L. Kalousek and A. F. Prebus, "Crystal Chemistry of Hydrous Calcium Silicates: III, Morphology and Other Properties of Tobermorite and Related Phases," *J. Am. Ceram. Soc.*, **41** [4] 124–32 (1958).

[2]D. S. Snell, "Review of Synthesis and Properties of Tobermorite, C-S-H(I), and C-S-H Gel," *J. Am. Ceram. Soc.*, **58** [7–8] 272–95 (1975).

[3]H. F. W. Taylor, "Proposed Structure for Calcium Silicate Hydrate Gel," *J. Am. Ceram. Soc.*, **69** [6] 464–7 (1986).

[4]P. Yu, R. J. Kirkpatrick, B. Poe, P. F. McMillan, and X. Cong, "Structure of Calcium Silicate Hydrate (C-S-H): Near-, Mid-, and Far-Infrared Spectroscopy," *J. Am. Ceram. Soc.*, **82** [3] 742–8 (1999).

[5]E. Bonaccorsi, S. Merlino, and A. R. Kampf, "The Crystal Structure of Tobermorite 14 Å (Plombierite), a C–S–H Phase," *J. Am. Ceram. Soc.*, **88** [3] 505–12 (2005).

[6]G. L. Kalousek, "Crystal Chemistry of Hydrous Calcium Silicates: I, Substitution of Aluminum in Lattice of Tobermorite," *J. Am. Ceram. Soc.*, **40** [3] 74–80 (1957).

[7]S. Diamond, "Coordination of Substituted Aluminum in Tobermorite," *J. Am. Ceram. Soc.*, **47** [11] 593–4 (1964).

[8]S. Yamazaki and H. Toraya, "Determination of Positions of Zeolitic Calcium Atoms and Water Molecules in Hydrothermally Formed Aluminum-Substiqtuted Tobermorite-1.1 nm Using Synchrotron Radiation Powder Diffraction Data," *J. Am. Ceram. Soc.*, **84** [11] 2685–90 (2001).

[9]S. Komarneni and M. Tsuji, "Selective Cation Exchange in Substituted Tobermorites," *J. Am. Ceram. Soc.*, **72** [9] 1668–74 (1989).

[10]M. Tsuji, S. Komarneni, and P. Malla, "Substituted Tobermorites: ^{27}Al and ^{29}Si MASNMR, Cation Exchange, and Water Sorption Studies," *J. Am. Ceram. Soc.*, **74** [2] 274–9 (1991).

[11]A. J. Qomi, F.-J. Ulm, R. Pellenq, and J.-M. Roland, "Evidence on the Dual Nature of Aluminum in the Calcium-Silicate-Hydrates Based on Atomistic Simulations," *J. Am. Ceram. Soc.*, **95** [3] 1128–37 (2012).

[12]T. Mitsuda, K. Sasaki, and H. Ishida, "Phase Evolution During Autoclaving Process of Aerated Concrete," *J. Am. Ceram. Soc.*, **75** [7] 1858–63 (1992).

[13]J. Kikuma, M. Tsunashima, T. Ishikawa, S.-Y. Matsuno, A. Ogawa, K. Matsui, and M. Sato, "In Situ Time-Resolved X-Ray Diffraction of Tobermorite Formation Process Under Autoclave Condition," *J. Am. Ceram. Soc.*, **93** [9] 2667–74 (2011).

[14]N. Isu, K. Sasaki, H. Ishida, and T. Mitsuda, "Mechanical Property Evolution During Autoclaving Process of Aerated Concrete Using Slag: I, Tobermorite Formation and Reaction Behavior of Slag," *J. Am. Ceram. Soc.*, **77** [8] 2088–92 (1994).

[15]N. Isu, S. Teramura, H. Ishida, and T. Mitsuda, "Mechanical Property Evolution During Autoclaving Process of Aerated Concrete Using Slag: II, Fracture Toughness and Microstructure," *J. Am. Ceram. Soc.*, **77** [8] 2093–6 (1994).

[16]K. Sasaki, T. Masuda, H. Ishida, and T. Mitsuda, "Structural Degradation of Tobermorite During Vibratory Milling," *J. Am. Ceramic Soc.*, **79** [6] 1569–74 (1996).

[17]R. Shahsavari, M. J. Buehler, R. J. M. Pellenq, and F.-J. Ulm, "First-Principles Study of Elastic Constants and Interlayer Interactions of Complex Hydrated Oxides: Case Study of Tobermorite and Jennite," *J. Am. Ceramic Soc.*, **92** [10] 2323–30 (2009).

[18]M. W. Barnes and B. E. Scheetz, "The Chemistry of Al-Tobermorite and its Coexisting Phases at 175°C"; pp. 243–71 in *Material Research Society Symposium Proceedings, Vol. 73, Specialty Cements with Advanced Properties*, Edited by B. E. Scheetz, A. G. Landers, I. Oder and H. Jennings. Materials Research Society, Warrendale, PA, 1991.

[19]T. Mitsuda and H. F. W. Taylor, "Normal and Anomalous Tobermorites," *Miner. Magazine*, **42**, 229–35 (1978).

[20]E. Bonaccorsi and S. Merlino, "Modular Microporous Minerals: Cancrinite-Davyne Group and C-S-H Phases," *Rev. Miner. Geochem.*, **57**, 241–90 (2005).

[21]S. Jakobsson and J. G. Moore, "Hydrothermal Minerals and Alteration Rates at Surtsey Volcano, Iceland," *Geol. Soc. Amer. Bull*, **97**, 648–59 (1986).

[22]S. Komarneni and D. Roy, "Tobermorites: A New Family of Cation Exchangers," *Science*, **221**, 647–8 (1983).

[23]S. Komarneni, E. Breval, M. Miyake, and R. Roy, "Cation-Exchange Properties of (Al + Na)-Substituted Synthetic Tobermorites," *Clays Clay Miner.*, **35** [5] 385–90 (1987).

[24]S. A. Hamid, "The Crystal Structure of the 11Å Natural Tobermorite $Ca_{2.25}[Si_3O_{7.5}(OH)_{1.5}] \cdot 1H_2O$)," *Z. Kristallogr.*, **154**, 189–98 (1981).

[25]S. Merlino, E. Bonaccorsi, and T. Armbruster, "The Real Structure of 11Å: Normal and Anomalous Forms, OD Character and Polytypic Modifications," *Eur. J. Miner.*, **13**, 577–90 (2001).

[26]A. Gmira, M. Zabat, R. Pellenq, and H. Van Damme, "Microscopic Physical Basis of the Poromechanical Behavior of Cement-Based Materials," *Mater. Struct.*, **37**, 3–14 (2004).

[27]H. Manzano, J. S. Dolado, A. Guerrero, and A. Ayuela, "Mechanical Properties of Crystalline Calcium-Silicate Hydrates: Comparison with Cementitious C-S-H Gels," *Physica Status Solidi (a)*, **204**, 1775–80 (2007).

[28]R. J. M. Pellenq, A. Kushima, R. Shahsavari, K. J. Van Vliet, M. J. Buehler, S. Yip, and F.-J. Ulm, "A Realistic Molecular Model of Cement Hydrates," *Proc. Natl Acad. Sci.*, **106**, 16102–7 (2009).

[29]F. Massazza, "Pozzolana and Pozzolanic Cements"; pp. 471–632 in *Lea's Chemistry of Cement and Concrete*, 4th edition, Edited by P. C. Hewlett, Arnold, London, 2004.

[30]G. K. Sun, J. F. Young, and R. J. Kirkpatrick, "The Role of Al in C–S–H: NMR, XRD, and Compositional Results for Precipitated Samples," *Cem. Concrete Res.*, **36**, 18–29 (2006).

[31]B. Lothenbach, K. Scrivener, and R. D. Hooton, "Supplementary Cementitious Materials," *Cem. Concrete Res.*, **41**, 217–29 (2011).

[32]J. P. Oleson, C. Brandon, S. M. Cramer, R. Cucitore, E. Gotti, and R. L. Hohlfelder, "The ROMACONS Project: A Contribution to the Historical and Engineering Analysis of Hydraulic Concrete in Roman Maritime Structures," *IJNA*, **33**, 199–229 (2004).

[33]G. Vola, E. Gotti, C. Brandon, J. P. Oleson, and R. L. Hohlfelder, "Chemical, Mineralogical and Petrographic Characterization of Roman Ancient Hydraulic Concrete Cores From Santa Liberata, Italy, and Caesarea Palestinae, Israel," *Per. Miner.*, **80**, 317–38 (2011).

[34]C. Stanislao, C. Rispoli, G. Vola, P. Cappelletti, V. Morra, and M. de Gennaro, "Contribution to the Knowledge of Ancient Roman Seawater Concretes: Phlegrean Pozzolan Adopted in the Construction of the Harbour at Soli-Pompeiopolis (Mersin, Turkey)," *Per. Miner.*, **80**, 471–88 (2011).

[35]M. D. Jackson, G. Vola, D. Všianský, J. P. Oleson, B. E. Scheetz, C. Brandon, and R. L. Hohlfelder, "Cement Microstructures and Durability in Ancient Roman Seawater Concretes"; pp. 49–76 in *Historic Mortars, Characteristics and Tests*, Edited by J. Valek, C. Groot and J. Hughes, Springer – RILEM, Berlin, 2012.

[36]C. Brandon, R. L. Hohlfelder, and J. P. Oleson, "The Concrete Construction of the Roman Harbours of Baiae and Portus Iulius, Italy: The ROMACONS 2006 Field Season," *IJNA*, **37**, 374–92 (2008).

[37]M. D. Jackson, S. R. Chae, S. R. Mulcahy, C. Meral, R. Taylor, P. Li, A.-H. Emwas, J. Moon, S. Yoon, G. Vola, H.-R. Wenk, and P. J. M. Monteiro, "Unlocking the Secrets of Al-Tobermorite in Roman Seawater Concrete," *Am. Miner.*, in press.

[38]P. K. Mehta, *Concrete in the Marine Environment*. Elsevier, New York, 1991.

[39]C. Langton and D. M. Roy, "Longevity of Borehole and Shaft Sealing Materials: Characterization of Ancient Cement Based Building Materials," *Mat. Res. Soc. Symp. Proc.*, **26**, 543–9 (1984).

[40]R. Sersale and P. G. Orsini, "Hydrated Phases After Reaction of Lime with Pozzolanic Materials or with Blast Furnace Slag," *Proc. 5th Symp. Chem. Cem.*, **4** [7] 114–21 (1969).

[41]W. L. Chao, B. D. Harteneck, J. A. Liddle, E. H. Anderson, and D. T. Attwood, "Soft X-ray Microscopy at a Spatial Resolution Better Than 15 nm," *Nature*, **435**, 1210–3 (2005).

[42]S. Rehbein, S. Heim, P. Guttmann, S. Werner, and G. Schneider, "Ultra High-Resolution Soft X-ray Microscopy with Zone Plates in High Orders of Diffraction," *Phys. Rev. Lett.*, **103**, 110801, 4pp (2009).

[43]J. Yang, Y. Yhang, and W. Yin, "A Fast Alternating Direction Method for TVL1-L2 Signal Reconstruction From Partial Fourier Data.hn IEEE," *Select Topics Signal Process*, **4**, 288–97 (2010).

[44]L. Pothuaud, P. Porion, E. Lespessailles, C. L. Benhamou, and P. Levitz, "A New Method for Three-Dimensional Skeleton Graph Analysis of Porous Media: Application to Trabecular Bone Architecture," *J. Microsc.*, **199** [2] 149–61 (2000).

[45]G. Schneider, P. Guttmann, S. Rehbein, S. Werner, and R. Follath, "Cryo X-ray Microscope with Flat Sample Geometry for Correlative Fluorescence and Nanoscale Tomographic Imaging.," *J. Struct. Biol.*, **177**, 212–23 (2012).

[46]S. R. Chae, J. Moon, S. Yoon, S. Bae, P. Levitz, R. Winarski, and P. J. M. Monteiro, "Advanced Nanoscale Characterization of Cement Based Materials Using X-ray Synchrotron Radiation: A Review," *Intl. J. Concrete Struct. Mater.*, in press, DOI 10.1007/s40069-013-0036-1.

[47]M. Han, S. Youssef, R. Rosenberg, M. Fleury, and P. Levitz, "Deviation From Archie's Law in Partially Saturated Porous Media: Wetting Film Versus Disconnectedness of the Conducting Phase," *Phys. Rev. E*, **79**, 031127, 11pp (2009).

[48]P. Levitz, V. Tariel, V. , M. Stampanoni, and E. Gallucci, "Topology of Evolving Pore Networks," *Eur. Phys. J. Appl. Phys.*, **60**, 24202, 9pp (2012).

[49]N. Tamura, M. Kunz, K. Chen, R. S. Celestre, A. A. MacDowell, and T. Warwick, "A Superbend X-Ray Microdiffraction Beamline at the Advanced Light Source," *Mat. Sci. Eng. A*, **524**, 28 (2009).

[50]M. Kunz, A. A. MacDowell, W. A. Caldwell, D. Cambie, R. S. Celestre, E. E. Domning, R. M. Duarte, A. E. Gleason, J. M. Glossinger, N. Kelez, D. W. Plate, T. Yu, J. M. Zaug, H. A. Padmore, R. Jeanloz, A. P. Alivisatos, and S. M. Clark, "A Beamline for High-Pressure Studies at the Advanced Light Source with a Superconducting Bending Magnet as the Source," *J. Synch. Rad.*, **12**, 650–8 (2005).

[51]H. K. Mao, J. Xu, and P. M. Bell, "Calibration of the Ruby Pressure Gauge to 800 Kbar Under Quasi-Hydrostatic Conditions," *J. Geophys. Res.*, **91**, 4673–6 (1986).

[52]A. P. Hammersley, S. O. Svensson, M. Hanfland, A. N. Fitch, and D. Housermann, "Two-Dimensional Detector Software: From Real Detector to Idealised Image or Two-Theta Scan," *High Pressure Res.*, **14**, 235–48 (1996).

[53]R. W. Cheary and A. A. Coelho, *"Programs XFIT and FOURYA", Deposited in CCP14 Powder Diffraction Library*. Engineering and Physical Sciences Research Council, Daresbury Laboratory, Warrington, England, 1996. http://wwwccp14acuk/tutorial/xfit-95/xfithtm.

[54]J. Laugier and B. Bochu, *Cell Parameter Refinement Program From Powder Diffraction Diagram*. CELREF. Version 3. Laboratoire des Matériaux et du Génie Physique, Ecole Nationale Supérieure de Physique de Grenoble (INPG), France, 2002.

[55]S. Merlino, E. Bonaccorsi, M. Merlini, F. Marchetti, and W. Garra, "Tobermorite 11Å and Its Synthetic Counterparts: Structural Relationships and Thermal Behaviour," *Miner. Adv. Mater.*; pp. 37–44 in *Minerals as Advanced Materials I*, Edited by S. Krivovichev. Springer-Verlag Berlin Heidelberg, (2008).

[56]S. Komarneni, R. Roy, D. Roy, C. A. Fyfe, G. J. Kennedy, A. A. Bothner-By, J. Dadok, and A. S. Chesnick, "^{27}Al and ^{29}Si Magic Angle Spinning Nuclear Magnetic Resonance Spectroscopy of Al-Substituted Tobermorites," *J. Mat. Sci.*, **20**, 4209–14 (1985).

[57]J. Houston, R. S. Maxwell, and S. A. Carroll, "Transformation of Meta-Stable Calcium Silicate Hydrates to Tobermorite: Reaction Kinetics and Molecular Structure From XRD and NMR Spectroscopy.," *Geochem. Trans.*, **10**, 1–14 (2009).

[58]J. Skibsted, H. Jakobsen, and C. Hall, "Direct Observation of Aluminum Guest Ions in the Silicate Phases of Cement Minerals by ^{27}Al MAS Spectroscopy," *J. Chem. Soc.*, **90**, 2095–8 (1994).

[59]I. G. Richardson and G. W. Groves, "The Incorporation of Minor and Trace Elements into Calcium Silicate Hydrate (C-S-H) Gel in Hardened Cement Pastes," *Cem. Concrete Res.*, **23**, 131–8 (1993).

[60]R. Taylor, I. G. Richardson, and R. M. D. Brydson, "Composition and Microstructure of 20-Year-old Ordinary Portland Cement–Ground Granulated Blast-Furnace Slag Blends Containing 0 to 100% Slag," *Cem. Concrete Res.*, **40**, 971–83 (2010).

[61]W. Wieker, A.-R. Grimmer, A. Winkler, M. Mägi, M. Tarmak, and E. Lippmaa, "Solid-State High-Resolution ^{29}Si Spectroscopy of Synthetic 14Å, 11 Å, and 9 Å Tobermorites," *Cem. Concrete Res.*, **12**, 333–9 (1992).

[62]L. B. Skinner, S. R. Chae, C. J. Benmore, H. R. Wenk, and P. J. M. Monteiro, "Nanostructure of Calcium Silicate Hydrates in Cements," *Phys. Rev. Lett.*, **104**, 195–202 (2010).

[63]G. D. Gatta, P. Cappelletti, N. Rotiroti, C. Slebodnick, and R. Rinaldi, "New Insights into the Crystal Structure and Crystal Chemistry of the Zeolite Phillipsite," *Am. Miner.*, **94**, 190–9 (2009).

[64]F. Massazza, "Concrete Resistance to Seawater and Marine Environment," *Il Cemento.*, **1**, 3–25 (1985).

[65]A. W. Walton and P. Schiffman, "Alteration of Hyaloclastites in the HSDP 2 Phase 1 Drill Core: 1. Description and Paragenesis," *Geochem. Geophys. Geosys.*, **4** [5] 1–31 (2003).

[66]F. Birch, "Finite Strain Isotherm and Velocities for Single-Crystal and Polycrystalline NaCl at High Pressures and 300K," *J. Geophys. Res.*, **83**, 1257–68 (1978).

[67]B. C. Reed, "Linear Least-Squares Fits with Errors in Both Coordinates," *Am. J. Phys.*, **57**, 642–6 (1989).

[68]C. T. Shannon, "Revised Effective Ionic Radii and Systematic Studies of Interatomic Distances in Halides and Chalcogenides," *Acta Cryst. Section A*, **32** [5] 751–67 (1976).

[69]J. E. Oh, S. M. Clark, and P. J. M. Monteiro, "Does the Al Substitution in C-S-H(I) Change Its Mechanical Property?" *Cem. Concrete Res.*, **41**, 102–6 (2011).

[70]R. M. Wentzcovitch, Y. G. Yu, and Z. Wu, "Thermodynamic Properties and Phase Relations in Mantle Minerals by First Principles Quasiharmonic Theory," *Rev. Miner. Geochem.*, **7** 1 59–98 (2010).

[71]S. Komarneni, "Phillipsite in Cs Decontamination and Immobilization," *Clays Clay Miner.*, **33** [2] 145–51 (1985).

[72]L. Trotignon, V. Devallois, H. Peycelon, C. Tiffreau, and X. Bourbon, "Predicting the Long Term Durability of Concrete Engineered Barriers in a Geological Repository for Radioactive Waste," *Phys. Chem. Earth, Parts A/B/C*, **32** [1–7] 259–74 (2007). □